A neoclassical calculation of toroidal rotation profiles and comparison with DIII-D measurements

W. M. Stacey, R. W. Johnson, and J. Mandrekas[a]
Fusion Research Center, Georgia Institute of Technology, Atlanta, Georgia 30332

Momentum and particle balance and neoclassical viscosity were applied to calculate the radial profile of toroidal rotation velocity in several DIII-D [J. Luxon, Nucl. Fusion **42**, 614 (2002)] discharges in a variety of energy confinement regimes (low-mode, low-mode with internal transport barrier, high-mode, and high-mode with quiescentd double barrier). Calculated toroidal rotation velocities generally were found to (over) predict measured values to well within a factor of 2. © 2006 American Institute of Physics. [DOI: 10.1063/1.2212391]

I. INTRODUCTION

There have been longstanding experimental[1–10] and theoretical[11–28] efforts to characterize and understand toroidal rotation and the related radial transport of angular momentum in neutral beam driven tokamaks. Since the theoretical expression for the toroidal rotation velocity follows directly from toroidal momentum balance once the viscous stress is specified, understanding toroidal rotation is primarily a matter of understanding toroidal viscosity (and any other torque input mechanisms).

It was noted earlier that the familiar PERPENDICULAR viscosity of classical theory was much too small to account for observed momentum damping,[1,13–15] even when extended to take neoclassical effects into account,[13–15,18,19] giving rise to the now widespread belief that momentum transport in tokamaks was "anomalous." The observation in several recent experimental investigations[4,5,7,8,10,29] that the ratio of the inferred momentum diffusivity and ion thermal diffusivity (χ_ϕ/χ_i), or the ratio of parameters that are determined by these diffusivities, was relatively uniform over the radial dimension of the plasma was interpreted as further evidence that the momentum transport was anomalous, since the ion thermal transport was believed to be anomalous in these discharges.

It was also pointed out early[11,12] (but little noted) that there was a second, GYROVISCOUS contribution to the radial transport of angular momentum in classical theory with a gyroviscosity coefficient that was several orders of magnitude larger than the perpendicular viscosity coefficient. The relative obscurity of the gyroviscous contribution in momentum transport analyses is perhaps due in part to the fact that it vanishes in cylindrical geometry (hence would not have survived in much of the early theoretical work) and in part by its puzzling failure to survive in some contemporary developments of neoclassical viscosity based on a formal gyroradius ordering of the flow fields,[18,19,26] all of which essentially recovered the much smaller classical perpendicular viscosity with small corrections. In any case, unfamiliarity notwithstanding, there would now appear to be a firm theoretical basis for gyroviscosity.[11,12,16,17,20–25,27,28] It is our purpose in this paper to test neoclassical viscosity by using neoclassical gyroviscosity to calculate the radial profile of toroidal rotation velocity and to use neoclassical parallel viscosity to calculate the poloidal rotation and the poloidal density and velocity asymmetries that are needed to evaluate the gyroviscous torque, and to compare the result with measured values of toroidal rotation in a set of DIII-D discharges.

We anticipate that there may be other, nonclassical momentum transport mechanisms present in DIII-D (and other) discharges (e.g., Ref. 30). However, since the particle motions and forces that give rise to classical and neoclassical transport are always present (trapped particle effects only in the appropriate collisionality regime), it is important to make a comparison of the predictions of neoclassical momentum transport theory with rotation measurements, if for no other reason than to establish the magnitude of the additional transport that must be accounted for by these other transport mechanisms.

For this purpose, we make use of the practical computation formalism that has been developed by extending the Braginskii gyroviscosity formalism to tokamak toroidal flux surface geometry[17] (i.e., the "Pfirsch-Schluter" extension of classical gyroviscosity) and by developing a methodology for evaluating the poloidal asymmetry factors needed to determine the rate of radial transport of toroidal angular momentum.[20] A number of previous, less extensive, comparisons of this formalism with experimental data[31–33] have established that gyroviscosity predicts the correct magnitude of the global momentum loss rate (the momentum confinement time) in many neutral beam driven tokamaks and under a variety of operating conditions. The intent of this paper is to extend these investigations to test the ability of this gyroviscosity formalism to predict the radial profile, as well as the overall magnitude, of the radial transport rate of toroidal angular momentum for neutral beam driven DIII-D plasmas in a variety of energy confinement regimes.

Radial momentum transport in tokamak plasmas is of intrinsic interest, of course, for what it reveals about basic transport processes. Moreover, toroidal rotation has also been shown to affect neoclassical particle transport,[34,35] to suppress MHD resistive wall mode instabilities,[36–38] and to alter

---

[a]On leave to the Office Fusion Energy Science, U. S. Department of Energy, Germantown, Maryland.

13, 062508-1

MHD equilibria,[39] and is postulated to be involved in the shear suppression of transport enhancing microinstabilities.[40]

II. NEOCLASSICAL RADIAL TRANSPORT OF TOROIDAL ANGULAR MOMENTUM

A. Viscous torques

Following the previous generalization[17] to toroidal flux-surface geometry of the Braginskii[12] derivation, the toroidal component of the viscous torque can be written

$$R^2 \nabla \phi \cdot \nabla \cdot \Pi = \frac{1}{Rh_p} \frac{\partial}{\partial l_\psi} (R^2 h_p \Pi_{\psi\phi}) + B_p \frac{\partial}{\partial l_p} \left(\frac{R\Pi_{p\phi}}{B_p} \right),$$

(1)

where the Π_{pq} are the stress tensor elements that result from the Braginskii decomposition of the rate-of-strain tensor extended to a right-hand "radial," "poloidal," toroidal (ψ, p, ϕ) flux-surface coordinate system with length elements $(dl_\psi = h_\psi d\psi, \ dl_p = h_p dp, \ dl_\phi = h_\phi d\phi)$. The viscous stress tensors have[17] "perpendicular" components

$$\Pi_{\psi\phi}^\perp = -\eta_2 R \frac{\partial}{\partial l_\psi} (V_\phi/R), \quad \Pi_{p\phi}^\perp = -\eta_2 R \frac{\partial}{\partial l_p} (V_\phi/R) \quad (2)$$

gyroviscous components

$$\Pi_{\psi\phi}^{gv} = -\eta_4 R \frac{\partial}{\partial l_p} (V_\phi/R), \quad \Pi_{p\phi}^{gv} = -\eta_4 R \frac{\partial}{\partial l_\psi} (V_\phi/R) \quad (3)$$

and "parallel" viscous components

$$\Pi_{\psi\phi}^\parallel = 0, \quad \Pi_{p\phi}^\parallel = -\tfrac{3}{2} \eta_0 f_p A_0, \quad (4)$$

where

$$A_0 = 2 \left\{ -\frac{1}{3} \left(\frac{\partial V_p}{\partial l_p} \right) + \left[\left(\frac{1}{R} \right) \frac{\partial R}{\partial l_p} + \frac{1}{3} \left(\frac{1}{B_p} \right) \frac{\partial B_p}{\partial l_p} \right] V_p \right. $$
$$\left. + f_p R \frac{\partial (V_\phi/R)}{\partial l_p} \right\} \quad (5)$$

and $f_p = B_p/B_\phi$.

The Braginskii values of the viscosity coefficients in a collisional plasma are

$$\eta_0 \simeq nT\tau, \quad \eta_4 \simeq nTm/ZeB = \eta_0/\Omega\tau,$$

(6)

$$\eta_2 \simeq \eta_4/\Omega\tau \simeq \eta_0/(\Omega\tau)^2,$$

where τ is the self-collision time and $\Omega = m/ZeB$ is the gyrofrequency. Since typically $\Omega\tau \approx 10^3 - 10^4$, $\eta_0 \gg \eta_4 \gg \eta_2$. Taking into account trapped particle effects that would occur at lower collisionality should not directly effect η_4, which has no τ dependence, and has been shown[18,19] to have very little effect on η_2. However, trapped particle effects at lower collisionality have a major effect on η_0, which we represent as[34]

$$\eta_{0j} = \frac{n_j m_j v_{thj} qR \varepsilon^{-3/2} \nu_{jj}^*}{(1 + \varepsilon^{-3/2} \nu_{jj}^*)(1 + \nu_{jj}^*)} \equiv n_j m_j v_{thj} qR f_j(\nu_{jj}^*), \quad (7)$$

where $\nu_{jj}^* = \nu_{jj} qR/v_{thj}$, v_{thj} is the thermal speed, q is the safety factor, and $\varepsilon = r/R$.

Since the flux surface average of the second term in Eq. (1) vanishes identically, and the "parallel" component of the first term in Eq. (1) vanishes identically, the flux surface averaged toroidal viscous torque may be written as the sum of the gyroviscous and perpendicular viscous components

$$\langle R^2 \nabla \phi \cdot \nabla \cdot \Pi \rangle = \langle R^2 \nabla \phi \cdot \nabla \cdot \Pi \rangle_{gv} + \langle R^2 \nabla \phi \cdot \nabla \cdot \Pi \rangle_\perp,$$

(8)

where

$$\langle R^2 \nabla \phi \cdot \nabla \cdot \Pi \rangle_{gv} = -\left\langle \frac{1}{Rh_p} \frac{\partial}{\partial l_\psi} \left(R^3 h_p \eta_4 \frac{\partial}{\partial l_p} (V_\phi/R) \right) \right\rangle$$

(9)

and

$$\langle R^2 \nabla \phi \cdot \nabla \cdot \Pi \rangle_\perp = -\left\langle \frac{1}{Rh_p} \frac{\partial}{\partial l_\psi} \left(R^3 h_p \eta_2 \frac{\partial}{\partial l_\psi} (V_\phi/R) \right) \right\rangle.$$

(10)

If the plasma rotated as a rigid body, $\Omega \equiv V_\varphi/R \neq \Omega(\psi, p)$, then both of these components of the viscous torque would vanish identically. It is departure from rigid body rotation in the flux surface, $\Omega = \Omega(p)$, that drives the gyroviscous torque, and departure from rigid body rotation radially, $\Omega = \Omega(\psi)$, that drives the perpendicular viscous torque. Although the radial departure of the toroidal rotation velocity from rigid body rotation is generally larger by an order of magnitude or more than the poloidal departure of the toroidal rotation velocity from rigid body rotation in the flux surface, the gyroviscosity coefficient is larger than the perpendicular viscosity coefficient by 3–4 orders of magnitude, $\eta_4 \approx (\Omega\tau)\eta_2 \approx (10^3 - 10^4)\eta_2$, so that the gyroviscous toroidal torque is generally a couple of orders of magnitude larger than the perpendicular toroidal viscous torque. We note again that it was the smaller, but more familiar, perpendicular toroidal viscous torque to which several authors were referring when they stated that the neoclassical viscosity is too small to account for experimentally observed rotation damping.

Finally, we further note that it has been suggested[23] that the above expression for the gyroviscous toroidal torque, which is based on the Braginskii development of the viscous stress tensor, may overestimate the momentum transport rate in regions of steep pressure gradients and low toroidal rotation (e.g., the plasma edge pedestal) because of the $V_\phi \sim v_{th}$ ordering of the Braginskii derivation.[12] Mikhailovskii and Tsypin[16] were the first, and Catto and Simakov[27] and Ramos[28] the most recent, to repeat the Braginskii derivation in the $V_\phi \ll v_{th}$ ordering. Braginskii's derivation, which is used in this paper, is valid if the fluid velocities in the directions perpendicular and parallel to **B** are larger than the diamagnetic velocity and the diamagnetic velocity multiplied by B_φ/B_p, respectively.[25] If this condition is not satisfied, then a heat flux term may be required also in the parallel, perpendicular, and gyroviscous torque expressions.[25,27] This "large rotation" condition for the validity of the Braginskii ordering appears to be valid over most of the radius for the discharges considered in this paper, as will be discussed later.

B. Toroidal viscous torque approximate representation

In order to obtain an approximate model for numerically evaluating the gyroviscous torque on each flux surface separately, we specialize in toroidal geometry, use the representations $B = B^0/(1 + \varepsilon \cos \theta)$, $R = R_0(1 + \varepsilon \cos \theta)$, replace the radial gradients in Eq. (9) by radial gradient scale lengths (e.g., $L_n^{-1} = -1/n \partial n/\partial r$), and expand the poloidal dependence of densities and velocities in a low-order Fourier series of the form

$$n_j(r, \theta) = n_j^{(r)}[1 + n_j^c(r)\cos \theta + n_j^s(r)\sin \theta] \qquad (11)$$

to obtain a representation of the toroidal gyroviscous torque in terms of an angular momentum transfer, or "drag," frequency, ν_{dj}

$$\langle R^2 \nabla \phi \cdot \nabla \cdot \boldsymbol{\pi}_j \rangle_{\mathrm{gv}} \simeq \frac{1}{2} \widetilde{\theta}_j G_j \frac{n_j m_j T_j}{e_j B_\phi} \frac{V_{\phi j}^0}{\overline{R}} \equiv R n_j m_j \nu_{dj} V_{\phi j}^0, \qquad (12)$$

where

$$\widetilde{\theta}_j \equiv (4 + \widetilde{n}_j^c) \widetilde{V}_{\phi j}^s + \widetilde{n}_j^s(1 - \widetilde{V}_{\phi j}^c)$$

$$= (4 + \widetilde{n}_j^c)(-(\hat{V}_{\theta j}/\hat{V}_{\phi j})(\widetilde{\Phi}^s + \widetilde{n}_j^s) + \widetilde{\Phi}^s(1 + (\hat{P}_j'/\hat{V}_{\phi j})))$$

$$+ \widetilde{n}_j^s((\hat{V}_{\theta j}/\hat{V}_{\phi j})(\widetilde{\Phi}^c + \widetilde{n}_j^c + 2) - \widetilde{\Phi}^c(1 + (\hat{P}_j'/\hat{V}_{\phi j}))) \qquad (13)$$

represents poloidal asymmetries and

$$G_j \equiv -\frac{r}{\eta_{4j} V_{\phi j}} \frac{\partial(\eta_{4j} V_{\phi j})}{\partial r} = r(L_n^{-1} + L_T^{-1} + L_V^{-1}) \qquad (14)$$

represents radial gradients. We have used the gyroviscosity coefficient $\eta_{4j} \approx n_j m_j T_j / e_j B$ and introduced the notation

$$\hat{V}_{\theta j} \equiv \frac{V_{\theta j}^0}{f_p \upsilon_{\mathrm{th}j}}, \quad \hat{V}_{\phi j} \equiv \frac{V_{\phi j}^0}{\upsilon_{\mathrm{th}j}}, \quad \hat{P}_j' \equiv \frac{1}{n_j^0 e_j B_\theta^0 \upsilon_{\mathrm{th}j}} \frac{\partial \overline{p}_j}{\partial r},$$

$$f_p \equiv \frac{B_\theta}{B_\phi}, \quad \widetilde{n}_j^{c/s} \equiv \frac{n_j^{c/s}}{\varepsilon}, \quad \widetilde{\Phi}^{c/s} \equiv \frac{\Phi^{c/s}}{\varepsilon} = \frac{n_e^{c/s}}{\varepsilon(e\Phi/T_e)} \qquad (15)$$

with the last relation following from electron momentum balance, and neglected radial gradients in the density asymmetry coefficients $n_j^{c,s}$. The radial gradient scale lengths needed to evaluate the G_j from Eq. (14) are taken from experiment in this paper. Φ is the electrostatic potential.

C. "Neoclassical" terminology and collisionality dependence of gyroviscosity

The terminology "neoclassical" is used differently by various authors, and the collisionality dependence of the neoclassical gyroviscosity is subtle, so a brief discussion of both is in order. Transport due to collisions in straight field-line geometry (e.g., cylinders) is referred to as "classical" transport. Kaufman[11] and Braginskii[12] worked out a "classical" theory of viscosity. In the more familiar case of Braginskii, the viscosity was derived from kinetic theory under the assumption of large collisionality and large rotation $V_\phi \sim \upsilon_{\mathrm{th}}$.

Extension of the "classical" Braginskii collisional transport to include the effects of toroidal geometry (i.e., Pfirsch-Schluter transport) is referred to in this paper, but not by all authors, as "neoclassical" transport. In general, collisional transport in toroidal geometry includes the "classical" transport plus the new Pfirsch-Schluter "neoclassical" transport effects due to the toroidal geometry. Since the latter effects are larger, the "classical" transport is usually neglected in toroidal geometry relative to the new Pfirsch-Schluter "neoclassical" transport, but it is still there (i.e., the forces producing it are still operable). Mikhailovskii and Tsypin,[16] Stacey and Sigmar,[17] and recently Catto and Simakov[27] extended "classical" viscosity theory to toroidal geometry to obtain what we refer to in this paper as a "neoclassical viscosity" theory that takes into account Pfirsch-Schluter-type toroidal geometry effects.

We note from Eq. (13) that this "Pfirsch-Schluter gyroviscosity" vanishes to leading order in the absence of an up-down asymmetry in either the density or the toroidal rotation velocity,[17] but survives at higher order.[27] This does not mean that gyroviscosity vanishes in a tokamak with an up-down symmetric magnetic field structure, because inertial and other effects can produce up-down density and rotation velocity asymmetries even in tokamaks with an up-down symmetric magnetic field structure.[20,31–33] Catto and Simakov[27] recently concluded purely on theoretical grounds that sufficiently strong up-down asymmetries such as that found in diverted plasmas could drive gyroviscous momentum transport rates comparable to those observed experimentally, but did not note that similarly strong up-down asymmetries could be produced by inertial and other effects (as our calculations will show). Relatively small poloidal asymmetries can cause a significant effect on radial momentum transport because $\eta_4 \approx (\Omega \tau) \eta_2 \approx (10^3 - 10^4) \eta_2$ and because the parallel viscosity contribution vanishes identically on the flux surface average.

At sufficiently small collisionality, trapped particle effects introduce additional transport effects in toroidal geometry that are usually larger than the Pfirsch-Schluter transport effects (at least for the more familiar heat conductivities), although the latter (and also the "classical" transport effects) are still present because most of the particles are untrapped. We refer to the transport associated with these trapped particle effects also as "neoclassical" transport, while noting that some authors refer to it as "banana-plateau" transport, and that yet other authors refer to only these trapped particle transport effects as "neoclassical." Numerous authors have investigated trapped particle effects on the parallel component of the viscosity tensor and found them to cause a significant enhancement of the viscosity coefficient [Eq. (7) is one such example], but of course to exist only when the collisionality was small enough to allow a small number of trapped particles to execute trapped particle orbits. Hinton and Wong[18] (and others) worked out the trapped particle effects on the perpendicular component of the viscosity and found only a small enhancement over the "classical" Braginskii value.

The Pfirsch-Schluter-type "neoclassical gyroviscosity" of this paper does not have any explicit collisionality depen-

dence, and no one has suggested that there is any direct trapped particle effect on gyroviscosity, to our knowledge. This does not mean that the Pfirsch-Schluter-type gyroviscosity does not exist in low collisionality plasmas, only that trapped particle effects do not directly enhance gyroviscosity relative to the "neoclassical Pfirsch-Schluter" values produced by toroidal geometry effects. However, since trapped particle effects enhance the parallel component of viscosity [Eq. (7)] that is used in solving the poloidal momentum moments equations [Eqs. (19)–(22)] for the poloidal velocities and density asymmetries needed to evaluate the gyroviscous torque from Eqs. (12)–(14), there is an indirect trapped particle collisionality dependence of gyroviscosity that is taken into account in the calculation of this paper.

D. Poloidal rotation velocities and density asymmetries

Evaluation of the poloidal asymmetry factors $\tilde{\theta}_j$ of Eq. (13) requires the solution of the poloidal momentum balance equations for the poloidal rotation velocities and the poloidal density asymmetries.

The poloidal component of the momentum balance equation is

$$n_j m_j [(V_j \cdot \nabla) V_j]_\theta + [\nabla \cdot \Pi_j]_\theta + \frac{1}{r}\frac{\partial p_j}{\partial \theta} - M_{\theta j} - F_{\theta j}$$

$$+ n_j e_j (V_{rj} B_\phi - E_\theta) = 0, \qquad (16)$$

where the poloidal components of the inertial and viscous terms are

$$n_j m_j [(V_j \cdot \nabla) V_j]_\theta = n_j m_j \left[V_{rj}\frac{\partial V_{\theta j}}{\partial r} + \frac{V_{rj}V_\theta}{r} + \frac{1}{2}\frac{1}{r}\frac{\partial V_{\theta j}^2}{\partial \theta} \right.$$

$$\left. + \frac{V_{\phi j}^2}{R}\sin\theta \right] \qquad (17)$$

and

$$[\nabla \cdot \Pi_j]_\theta = \eta_{0j}\left(\frac{1}{2}A_{oj}\right)\left\{ \frac{1}{r}\frac{\partial \ln(\eta_{0j}A_{oj})}{\partial \theta} - 3\frac{\sin\theta}{R}\right\} \qquad (18)$$

and M and F represent external momentum input from the neutral beam injection and interspecies collisional friction, respectively. We note that the "parallel" component of the viscosity enters the rotation calculation at this point and ultimately affects the calculation of the poloidal asymmetry factors $\tilde{\theta}_j$ which enter into the calculation of the frequencies ν_{dj} for the radial transport of toroidal angular momentum.

Making expansions of the type indicated by Eq. (11) for the density and velocities for each species in Eq. (16) and taking the flux surface average with weighting functions 1, $\sin\theta$ and $\cos\theta$ results in a coupled set of moments equations (three times the number of ion species) that must be solved for the $V_{\theta j}^0$ and $\tilde{n}_j^{s,c}$ for all the plasma ion species. If the first term on the right-hand side in Eq. (17) is neglected, these equations can be solved locally on each radial flux surface. The justification for this neglect is the plausible assumption $V_{rj} \ll V_{\theta j} < V_{\phi j}$. The resulting equations are

$$\hat{V}_{\theta j}\left[-q\hat{V}_{\phi j}\varepsilon(\tilde{n}_j^s + \tilde{\Phi}^s) - q^2 f_j f_p\left(1 + \tilde{\Phi}^c + \frac{2}{3}\tilde{n}_j^c\right) + f_p\sum_{k\neq j}\nu_{jk}^*(1 + \Delta_{\text{fric},j})\right] - \sum_{k\neq j}\hat{V}_{\theta k}\left[f_p\nu_{jk}^*\sqrt{\frac{m_j}{m_k}}\right](1 + \Delta_{\text{fric},k})$$

$$= -\hat{V}_{rj}(1 + \Delta_r) - q\varepsilon\frac{1}{4}\tilde{n}_j^s - q\varepsilon\hat{\Phi}_j\left[\frac{1}{4}(\tilde{\Phi}^s + \Delta_{\Phi j})\right] - q^2 f_j f_p(\hat{V}_{\phi j} + \hat{P}_j')\tilde{\Phi}^c - q\varepsilon\hat{V}_{\phi j}\left[(\hat{V}_{\phi j} + \hat{P}_j')\tilde{\Phi}^s + \frac{1}{2}\hat{V}_{\phi j}\tilde{n}_j^s\right], \qquad (19)$$

where $\Delta_{\text{fric},j} \equiv -\frac{1}{2}\varepsilon^2(1 + n_j^c + (n_j^c)^2 + (n_j^s)^2)$, $\Delta_{\Phi j} \equiv \tilde{n}_j^c\tilde{\Phi}^s - \tilde{n}_j^s\tilde{\Phi}^c$, Δ_r is a higher order term that arises from the second term in Eq. (17), and

$$\tilde{n}_j^s\left[\frac{1}{3}\frac{q^2}{\varepsilon}f_j f_p\hat{V}_{\theta j} + \frac{1}{2}\varepsilon\hat{V}_{rj} - \frac{1}{2}\varepsilon f_p\sum_{k\neq j}\nu_{jk}^*\hat{V}_{\theta k}\sqrt{\frac{m_j}{m_k}}\right]$$

$$+ \tilde{n}_j^c\left[\frac{1}{2}q f_p\hat{V}_{\theta j}^2 - \frac{1}{4}q\right]$$

$$= -\frac{1}{2}\varepsilon f_p\sum_{k\neq j}\nu_{jk}^*\hat{V}_{\theta j}\tilde{n}_k^s - \frac{1}{2}q\hat{V}_{\phi j}^2 + \frac{1}{4}q\hat{\Phi}_j\bar{\Phi}^c$$

$$- \frac{q^2}{\varepsilon}f_j f_p\frac{1}{2}(\hat{V}_{\theta j} - \hat{V}_{\phi j} - \hat{P}_j')\tilde{\Phi}^s - \frac{1}{2}q f_p^2\hat{V}_{\theta j}^2 + \Delta_{1,j},$$

$$\qquad (20)$$

where $\Delta_{1,j}$ is a collection of higher order terms calculated with a symbolic algebra routine, and

$$\tilde{n}_j^c\left[\frac{1}{3}\frac{q^2}{\varepsilon}f_j f_p\hat{V}_{\theta j} + \frac{1}{2}\varepsilon\hat{V}_{rj} - \frac{1}{2}\varepsilon f_p\sum_{k\neq j}\nu_{jk}^*\hat{V}_{\theta k}\sqrt{\frac{m_j}{m_k}}\right]$$

$$+ \tilde{n}_j^s\left[-\frac{1}{2}q f_p\hat{V}_{\theta j}^2 + \frac{1}{4}q\right]$$

$$= -\frac{1}{2}\varepsilon f_p\sum_{k\neq j}\tilde{n}_k^c[\nu_{jk}^*\hat{V}_{\theta j}] - \frac{1}{4}q\hat{\Phi}_j\tilde{\Phi}^s - \frac{q^2}{\varepsilon}f_j f_p$$

$$\times\left[\frac{1}{2}\{(1 + \tilde{\Phi}^c)\hat{V}_{\theta j} - (\hat{V}_{\phi j} + \hat{P}_j')\tilde{\Phi}^c\}\right] + \Delta_{2,j}, \qquad (21)$$

where $\Delta_{2,j}$ is a collection of higher order terms calculated with a symbolic algebra routine. The $\tilde{V}_{\phi j}^{s,c}$ are derived from

the radial component of the momentum balance equation and defined in Eq. (13) and in Eq. (25) below. We note that $V_{\theta j}^c/V_{\theta j}^0 = -\varepsilon(1 + \tilde{n}_j^c)$ and $V_{\theta j}^s/V_{\theta j}^0 = -\varepsilon(\tilde{n}_j^s)$ have been derived from the particle continuity equations and used in the above development. We have introduced the additional notation

$$\hat{V}_{rj} \equiv \frac{\bar{V}_{rj}}{\left(\frac{m_j v_{\mathrm{th}j}}{e_j B_\theta^0}\right)|f_p|\left(\frac{v_{\mathrm{th}j}}{qR}\right)}, \quad \nu_{jk}^* \equiv \frac{\bar{\nu}_{jk}}{\frac{v_{\mathrm{th}j}}{qR}}, \quad \hat{\Phi}_j \equiv \frac{e_j \bar{\Phi}}{T_j}.$$

$$(22)$$

The Δ_{xx} in Eqs. (19)–(21) are higher order terms that were not consistently retained in earlier versions (e.g., Ref. 24) of these equations.

E. Radial electric field and toroidal rotation velocities

For each ion species, the momentum balance equation minus $m_j \mathbf{V}_j$ times the particle balance equation is

$$n_j m_j (\mathbf{V}_j \cdot \nabla) \mathbf{V}_j + \nabla p_j + \nabla \cdot \Pi_j$$
$$= -n_j e_j \nabla \Phi + n_j e_j \mathbf{V}_j \times \mathbf{B} + \mathbf{F}_j + \mathbf{M}_j,$$

$$(23)$$

where $\mathbf{F}_j = -n_j m_j \nu_{jk}(\mathbf{V}_j - \mathbf{V}_k)$ is the interspecies collisional friction and $\mathbf{M}_j$ is the net external momentum input (e.g., neutral beam input less any charge-exchange and asymmetric ionization source losses). The lowest-order radial component of the flux surface average of Eq. (23) for each species j is

$$(\bar{E}_r/B_\theta^0) = V_{\phi j}^0 - (B_\phi^0/B_\theta^0)V_{\theta j}^0 + \bar{P}_j' + \bar{I}_j,$$

$$(24)$$

where the overbar or zero superscript indicates the average value over the flux surface. If the inertial term is retained in the radial momentum balance, there is an additional term on the right-hand side of Eq. (24) $\bar{I}_j \equiv (m/e)((V_{\theta j}^0)^2/r)$ but this term is generally higher order. We will include it in the calculation of toroidal rotation velocities [Eq. (32)], but since it is not used to construct the "experimental" electric field we will not include it in the calculation of radial electric field for comparison with experiment.

The lowest-order radial component of the flux surface average of the sin θ and cos θ moments of Eq. (23) can be solved for the toroidal rotation asymmetry factors when an expansion $V_{\phi j}(r, \theta) = V_{\phi j}^0(r)(1 + V_{\phi j}^c \cos\theta + V_{\phi j}^s \sin\theta)$ is made

$$\tilde{V}_{\phi j}^c = 1 - \left(\frac{\hat{V}_{\theta j}}{\hat{V}_{\phi j}}\right)(\tilde{\Phi}^c + \tilde{n}_j^c + 2) + \tilde{\Phi}^c\left(1 + \frac{\hat{P}_j'}{\hat{V}_{\phi j}}\right),$$

$$(25)$$

$$\tilde{V}_{\phi j}^s = \left(\frac{\hat{V}_{\theta j}}{\hat{V}_{\phi j}}\right)(\tilde{\Phi}^s + \tilde{n}_j^s) + \tilde{\Phi}^s\left(1 + \frac{\hat{P}_j'}{\hat{V}_{\phi j}}\right),$$

where $\tilde{V}_{\iota j}^{s,c} = V_{\iota j}^{s,c}/\varepsilon$. The lowest-order radial component of the flux surface average of the sin θ and cos θ moments of Eq. (23) for the electrons can be solved for electrostatic potential asymmetry factors when a similar expansion is made

$$\tilde{\Phi}^{c/s} \equiv \frac{\Phi^{c/s}}{\varepsilon} = \frac{n_e^{c/s}}{\varepsilon(e\Phi^0/T_e)}.$$

$$(26)$$

The flux surface average of the toroidal component of Eq. (23) for each species j can be written

$$n_j^0 m_j \bar{\nu}_{jk}((1 + \beta_j)V_{\phi j}^0 - V_{\phi k}^0) = n_j^0 e_j E_\phi^A + e_j B_\theta^0 \Gamma_j + \bar{M}_{\phi j}$$
$$\equiv n_j^0 m_j \bar{\nu}_{jk} y_j,$$

$$(27)$$

where radial transport of toroidal momentum is represented by the parameter

$$\beta_j \equiv \frac{\bar{\nu}_{dj} + \nu_{nj} + S_{nbj}/n_j^0}{\bar{\nu}_{jk}},$$

$$(28)$$

where S_{nbj} is the local neutral beam source rate, which arises because of use of the continuity equation in evaluating the inertial term, and the gyroviscous angular momentum transport frequency, ν_{dj}, is defined by Eq. (12) and the inertial angular momentum transport frequency, ν_{nj}, is defined by

$$\langle R^2 \nabla \phi \cdot n_j m_j (\mathbf{V}_j \cdot \nabla)\mathbf{V}_j\rangle$$
$$\simeq \frac{1}{2}\Bigg(\frac{V_{rj}}{R_o}\{\varepsilon(1 + \tilde{n}_j^c + \tilde{V}_{\phi j}^c) - 2R_o L_{\nu\phi,j}^{-1}\}$$
$$- \varepsilon\frac{V_{\theta j}^0}{R_o}\{\tilde{V}_{\phi j}^s(1 + \tilde{n}_j^c + \tilde{V}_{\phi j}^c)$$
$$- \tilde{V}_{\theta j}^s(1 + \tilde{V}_{\phi j}^c) - \tilde{V}_{\phi j}^c \tilde{n}_j^s\}\Bigg)n_j m_j R V_{\phi j}^0$$
$$\equiv R n_j m_j \nu_{nj} V_{\phi j}^0.$$

$$(29)$$

The ion-electron friction term has been neglected. A sum over other species k is implied and the collisional momentum conservation requirement $n_j^0 m_j \bar{\nu}_{jk} = n_k^0 m_k \bar{\nu}_{kj}$ has been used in deriving Eq. (27).

We note that most neoclassical derivations (e.g., Refs. 14 and 27) obtain the result that the radial electric field is proportional to the radial ion temperature gradient (which is proportional to V_θ in those derivations). The above equations can be rearranged to compare with these earlier derivations. Using the radial momentum balance Eq. (24) (but dropping the inertial terms) in the toroidal momentum balance Eqs. (27) to eliminate the $V_{\phi j}^0$ and summing over species yields another expression for the radial electrostatic field

$$\frac{\bar{E}_r}{B_\theta^0} = \frac{[\{\hat{M}_{\phi I} + \hat{M}_{\phi i}\} + \beta_i\{\bar{P}_i' - (B_\phi^0/B_\theta^0)(V_{\theta i}^0)\} + \beta_I\{\bar{P}_I' - (B_\phi^0/B_\theta^0)(V_{\theta I}^0)\}]}{[\beta_i + \beta_I]}$$

$$(30)$$

TABLE I. Parameters of DIII-D shots selected for rotation analysis.

Shot (time)	Conf. mode	P_{nbi} (MW)	$\bar{n}$ ($10^{19}/m^3$)	n_{carb}/n_e	(n_{neon}/n_e)	$(n_{ni,cu}/n_e)$	T_{i0}, T_{e0} (keV)	τ_E^{exp} (ms)
98777 1.6 s	L	4.5 CO	3.4	0.011	$\cdots$	$\cdots$	3.5, 2.5	66
98775 1.6 s	L	4.5 CO	4.1	0.005	0.028	$\cdots$	6.3,3.3	90
99411 1.8 s	H	9.2 CO	4.8	0.050	$\cdots$	$\cdots$	8.3, 3.9	168
106919 3.5s	H- QDB	9.3 CTR	2.8	0.037	$\cdots$	0.005	14.2, 4.2	140
106972 2.9s	H- QDB	8.7 CTR	2.9	0.031	0.003	0.003	15.2, 4.2	117
102942 1.4 s	L- ITB	7.0 CO	2.9	0.016	$\cdots$	$\cdots$	12.0, 4.7	94
102940 1.4 s	L- ITB	7.0 CO	3.2	0.006	0.013	$\cdots$	9.7, 4.1	128

that displays the dependence on momentum input, pressure, and poloidal rotation velocity. Since earlier derivations usually do not take into account the presence of external angular momentum input they naturally do not obtain the terms in the first brackets.

III. COMPARISON WITH DIII-D ROTATION MEASUREMENTS

The main purposes of this paper are to compare theoretical and experimental toroidal rotation velocity radial profiles and to draw some conclusions therefrom about how much of the radial transport of toroidal angular momentum in DIII-D tokamak plasmas is accounted for by neoclassical viscosity (as represented in the previous section) and how much must be attributed to other processes. A diverse set of discharges including *L* and *H* modes, with and without internal transport barriers and with and without neon injection, were analyzed for this purpose, as indicated in Table I. A secondary purpose was to extend the investigation of the effect of neon impurity injection on momentum transport, for which purpose three "sister shot" pairs with and without neon injection were included. The toroidal rotation measurements were made with charge-exchange recombination spectroscopy.

A. Description of discharges

L mode "sister shots" 98777 and 98775 at 1.6 s:[41]

These were *L* mode shots that were operated identically in every respect except for the injection of 2.8% neon impurity concentration in shot 98775. Long wavelength turbulence as well as heat and momentum transport were measured to be reduced with neon injection. The intrinsic carbon concentrations were 1.1% in 98777 and 0.5% in the neon injected 98775. (The cited carbon and neon concentrations correspond to the measured values at $\rho = \frac{1}{2}$ in this and other shots.)

L mode ITB "sister shots" 102942 and 102940 at 1.4 s:[42]

These were co-injected shots with an internal transport barrier (ITB) and a typical *L* mode edge. The measured temperature and toroidal velocity profiles were quite peaked throughout the discharge. The density profiles were flat early in the discharge, but sharp density and electron temperature gradients developed later in the discharge following an increase in beam power, indicating the formation of an internal transport barrier (ITB). The shots were operated identically except for neon injection in shot 102940, which produced broader profiles and higher temperatures (i.e., better energy confinement), larger toroidal rotation velocities, and reduced turbulence levels in the core as compared to the sister shot 102942 without neon injection.

H mode shot 99411 at 1.8 s:[43]

This was a high performance ($H_{89P}=2.8$, $\beta_N H_{89P}=10$) ELMing *H* mode shot with a typical *H* mode edge pedestal and a relatively large (5%) carbon intrinsic impurity concentration.

H mode QDB "sister shots" 106919 at 3.5 s and 106972 at 2.9 s:[44]

These were counterinjected, quiescent double barrier (QDB) shots with both an internal transport barrier and an edge transport barrier typical of *H* mode discharges. The edge was quiescent [i.e., free of edge localized modes (ELMs)], but a saturated coherent MHD edge harmonic oscillation (EHO) was present at the separatrix. The turbulence was reduced but not entirely suppressed in the internal transport barrier. These discharges had relatively low plasma densities and large and accumulating concentrations of Ni and Cu (Z_{eff} at $\rho = \frac{1}{2}$ was 4.1 at 2010 ms and 5.4 at 3510 ms, more than half of which was due to Ni and Cu). The carbon concentration was 3.7% in 106919 and 3.1% in 10697. The shots were operated identically except for neon injection in shot 106972.

B. "Two-species" calculation model

The calculation model consisted of Eqs. (19)–(21) for the poloidal rotation velocities and density asymmetries for the main ion (deuterium) and an effective impurity ion species, the two Eqs. (27) for the toroidal rotation velocities for the main and effective impurity ion species, and the radial component Eq. (24) of the momentum balance. We add the two toroidal momentum balance Eqs. (27) to obtain one relation between the deuterium and impurity ion rotation velocities

$$\beta_i V_{\phi i}^0 + \beta_I V_{\phi I}^0 = y_i + y_I \tag{31}$$

and then subtract the radial momentum balance Eq. (24) for the deuterium ion and effective impurity ion species to obtain a second relation

$$V_{\phi i}^0 - (B_\phi^0/B_\theta^0)V_{\theta i}^0 + \bar{P}_i' + I_i = V_{\phi I}^0 - (B_\phi^0/B_\theta^0)V_{\theta I}^0 + \bar{P}_I' + I_I. \tag{32}$$

The radial electric field then calculated from the radial momentum balance Eq. (24) for either the effective impurity species (consistent with the way the experimental radial electric field was calculated) or the main deuterium ion species were identical.

C. Evaluation of input parameters

We took the electron density distribution, the ion and electron temperature distributions, the toroidal electric field, and the radial gradient scale lengths L_n^{-1}, L_T^{-1}, and L_v^{-1} from experiment. The radial distribution of neutral beam angular momentum deposition was calculated with the code NBEAMS.[45] The value of the electrostatic potential Φ used in Eq. (19) to calculate the poloidal rotation velocity was taken from TRANSP calculations[46] based on an integration inward of the experimental radial electric field. The calculation was only made out to $\rho=0.9$ or 0.95 because atomic physics effects (not taken into account in the calculation) become an important momentum transfer mechanism closer to the separatrix.

A brief discussion of the use of the experimental radial gradient scale lengths L_n^{-1}, L_T^{-1}, and L_v^{-1} is in order at this point so that their effect on the calculation is clear. Our intent in this paper is to test the validity of Eq. (9) and its approximate representation Eq. (12), the expression for the gyroviscous torque which determines the rate of radial transport of toroidal angular momentum. The radial derivatives enter Eq. (12) via the factor G_j. We are not able at this time to accurately calculate the radial distributions of n, T, and V_φ needed to accurately evaluate G_j, yet the accurate evaluation the G_j is a necessary (but not sufficient) condition for Eq. (12) to predict the correct momentum transport rate. So we use the experimental gradient scale lengths to insure that an accurate evaluation of G_j is used to test Eq. (12). To put it another way, to calculate the correct momentum transport rate it is not only necessary to use the correct G_j, but also that the equation it is used in is the correct equation; e.g., if Eq. (10) for the perpendicular viscosity with $\eta=\eta_2 =(nmT/ZeB)/\Omega\tau$ was used instead of Eq. (9) to represent the

radial transport of toroidal angular momentum, and if the same experimental radial gradient scale lengths were used to evaluate the expression equivalent to Eq. (12) derived from Eq. (10), the resulting magnitude of the toroidal rotation velocity would be several orders of magnitude larger because $\Omega\tau \approx 10^3 - 10^4$.

In a similar vein, we have elected to use the value of the electrostatic potential Φ calculated in TRANSP by integrating the experimental radial electric field, rather than integrating the calculated radial electric field, because there is some ambiguity about the boundary conditions that should be used that probably outweighs any difference.

D. Modeling of multiple impurity species

Since the present model is limited (by implementation, not inherently) to two ion species—"main ion" and "impurity"—it was necessary to model the six charge states of carbon as a single impurity species with effective charge and mass determined by density weighting. This should be a good approximation over most of the plasma where carbon is fully ionized, but not in the edge. When neon was present it was similarly treated, and then the effective neon and carbon species were combined into a single effective impurity species. In the counterinjected shots with significant Cu and Ni impurities a similar treatment was used to obtain a single high Z (Ni+Cu) impurity that was then combined with carbon and neon to obtain a single effective impurity species. Clearly, the association of the calculated "impurity" rotation velocity with the measured carbon VI rotation velocity in the presence of neon and high Z impurities is valid only to the extent that the various impurity ion species are entrained by interspecies collisions to have a common rotation velocity, which is thus an implicit (and probably not very good) assumption of this model. We plan to introduce a multiple impurity species model in future work. Note that the less collisional main (deuterium) ions are not assumed to have the same rotation velocities as the more collisional impurity ions.

E. Numerical solution

Taking Eqs. (19)–(21) (for each species) and Eqs. (31) and (32) as our model for a two-species plasma of ions and impurities, we have an eight-dimensional system of coupled nonlinear equations at each radial mesh point. We solved this set of nonlinear equations for the rotation velocities and poloidal density coefficients ($V_{\phi i}$, $V_{\phi I}$, $V_{\theta i}$, $V_{\theta I}$, n_i^c, n_I^c, n_i^s, n_I^s) at each spatial location numerically, using standard procedures based on the simplex search algorithm[47,48] to minimize a scalar residual merit function defined as the magnitude of the sum of the normalized root-mean-square residuals for the individual equations at that spatial location. A convergence tolerance of $O(10^{-5})$ on the final step size in the change in the solution vector was used to define solutions, except as noted in the following section.

In general, more than one solution was found that satisfied this convergence criterion (depending on the initial trial solution), as is to be expected for a coupled set of nonlinear equations and an unrestricted search algorithm. Solutions
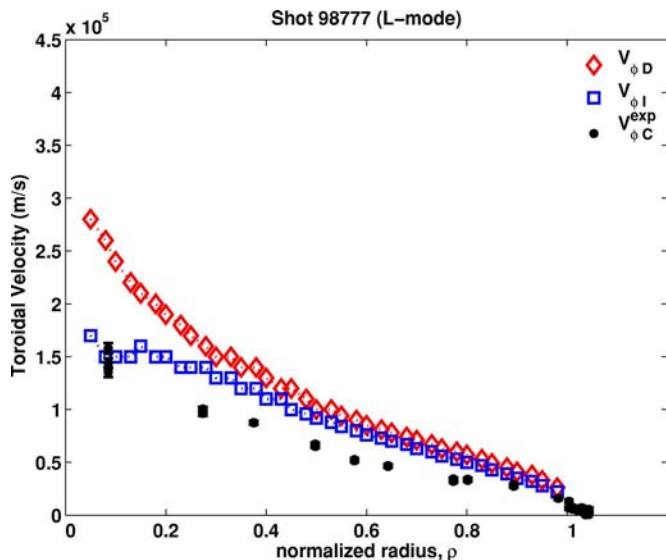
FIG. 1. Comparison of calculated and measured toroidal rotation velocities for the *L* mode shot 98777 without neon.

FIG. 2. Comparison of calculated and measured toroidal rotation velocities for the *L* mode shot 98775 with neon.

with scalar residuals up to a few percent (the estimated inaccuracy of the equations due to ancillary modeling approximations and input data uncertainties) were accepted. In some cases solutions were accepted at isolated radial locations with a somewhat larger scalar residual when they were an obvious continuation of the solution at nearby radial locations with smaller scalar residuals. The most physically plausible solution (e.g., the solution with density asymmetries everywhere less than the average density, hence everywhere positive density) meeting these criteria was selected as the physical solution.

F. Comparison of calculated and measured toroidal rotation velocities

The measured and calculated toroidal rotation frequencies are compared in Figs. 1–7. The calculated velocities are for the deuterium main ion species and for an effective impurity species, while the measured rotation velocity is for carbon VII. We generally found that the calculated deuterium velocity was somewhat greater than the calculated impurity velocity in the center, but that the difference diminished with radius. The calculated impurity species rotation velocity should be compared with the experimental carbon VII rotation velocity.

For the *L* mode shots in Figs. 1 and 2, the two calculated velocities were very similar at the outer radii but diverged at smaller radii, and the calculated impurity velocity was in quite good agreement with the measured values over the entire minor radius. Since only carbon impurity was present in shot 98777 and this impurity was fully ionized over most of the radius the single impurity species approximation should be valid, and the comparison of $V_{\phi I}$ and $V_{\phi C}^{exp}$ is an unambiguous test of the theory within the uncertainty introduced by geometric and other ancillary modeling approximations and the uncertainty in the input experiment density and temperature data. With shot 98775, the necessity (at this stage in the development of the calculation model) of treating neon and
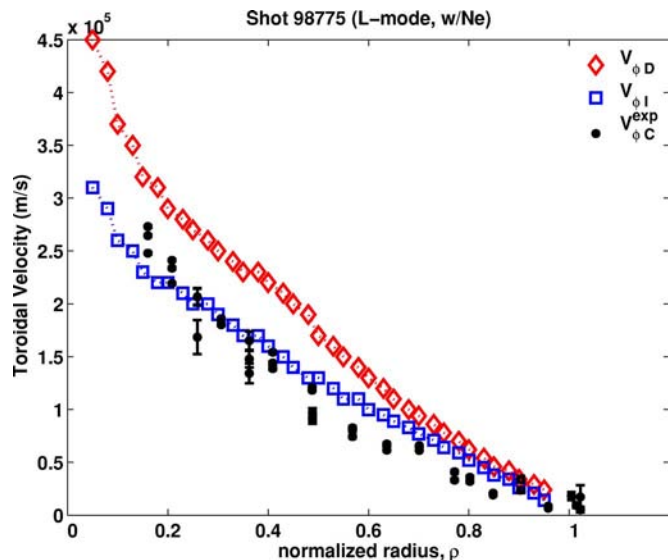
carbon as a single impurity species introduces an additional ambiguity into the comparison of $V_{\phi I}$ and $V_{\phi C}^{exp}$, which may account for the calculated impurity velocity falling below the measured carbon VII velocity in the center.

For the *L* mode shots with an ITB (just inside $\rho=0.4$) in Figs. 3 and 4, the calculated velocities for the impurity species were similar to those for deuterium except inside the location of the ITB, and generally in agreement with the measured values to within less than a factor of 2 (overprediction) at all radii. The same remarks made above about the single impurity species approximation apply also to this pair of shots.

For the *H* mode shot in Fig. 5 the calculated carbon velocity was in quite good agreement (slight overprediction) at all radii with the measured carbon VII velocity, and the
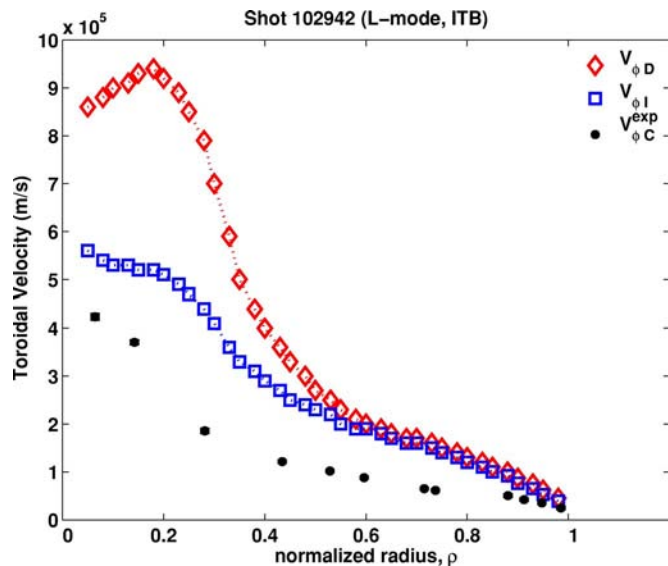

FIG. 3. Comparison of calculated and measured toroidal rotation velocities for the *L* mode shot 102942 with ITB but without neon.
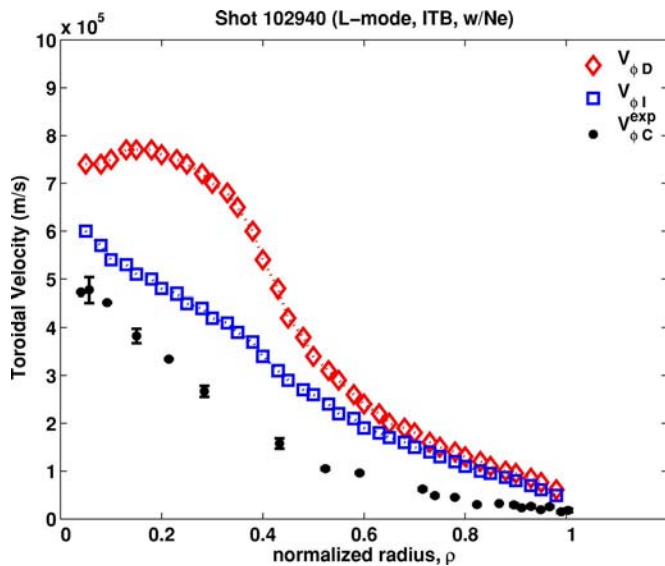
FIG. 4. Comparison of calculated and measured toroidal rotation velocities for the *L* mode shot 10940 with ITB and with neon.

FIG. 6. Comparison of calculation and measured toroidal rotation velocities for the *H* mode QDB shot 106919 without neon.

calculated deuterium velocity was larger than the calculated carbon velocity. Since carbon was the only impurity present, the comparison of $V_{\phi I}$ and $V_{\phi C}^{exp}$ provides an unambiguous test of the theory within the uncertainty introduced by geometric and other ancillary modeling approximations and the uncertainty in the input experiment density and temperature data.

For the lower density, counterinjected QDB shots with both an *H* mode edge and an ITB, it was not possible to find solutions with a convergence tolerance of $O(10^{-5})$ on the change in the final step size of the solution vector, and this tolerance was relaxed to $O(10^{-3})$ in order to obtain solutions. Even with this tolerance, the solutions were outside the physically reasonable range $|n_{i,1}^{c,s}| < 1$ except in the center region for shot 106919, and these density asymmetries were also implausibly large but less than unity in magnitude in shot 106972. The calculated deuterium velocities were sig-
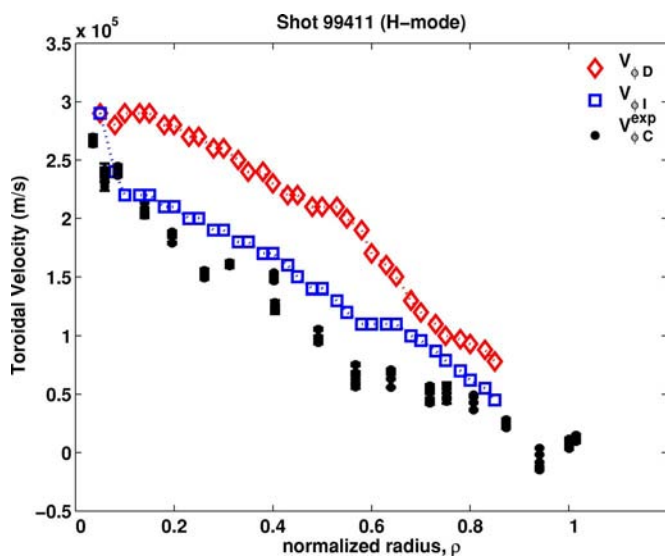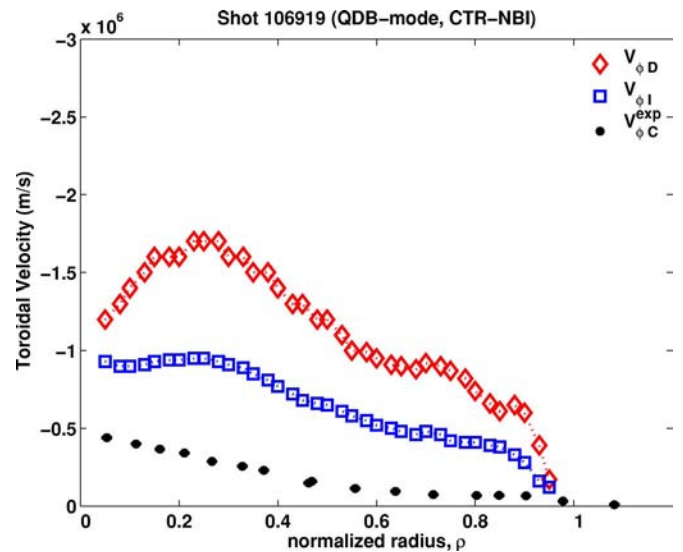
nificantly greater than the calculated impurity velocities at all but the outermost radii, and the calculated impurity velocity was generally about a factor of 2 larger than the measured carbon VII velocity. We attribute this behavior to a breakdown in the ancillary "one effective impurity species" approximation in which carbon, neon and several charge states of copper and nickel (the latter contributing about half the $Z_{eff} \approx 4$) were lumped together as a single impurity species. Even with these difficulties in the impurity representation model, agreement between calculated impurity and measured carbon VI velocities was within a factor of about 3. We note that differences in trace impurity toroidal velocities have been measured and calculated [using Eq. (32) but for two trace impurities] in DIII-D.[49]

In the "sister shot" pair of *L* mode shots that differed only by neon injection (98777 and 98775), both the mea-

FIG. 5. Comparison of calculated and measured toroidal rotation velocities for the *H* mode shot 99411.
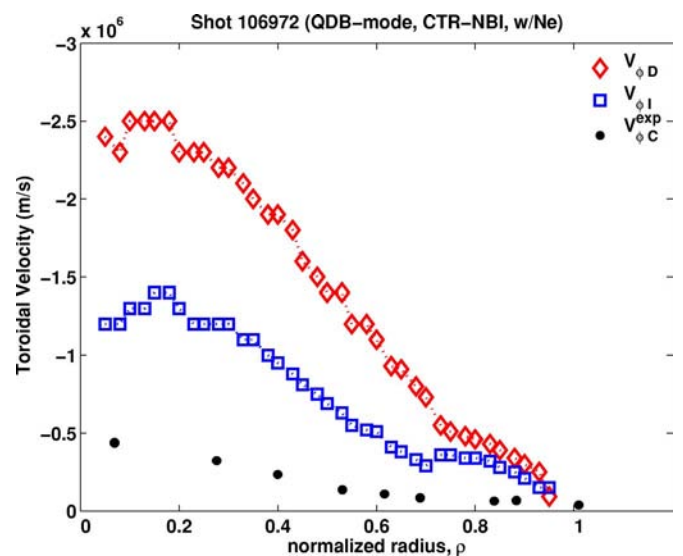

FIG. 7. Comparison of calculation and measured toroidal rotation velocities for the *H* mode QDB shot 106972 with neon.

sured and calculated rotation velocities were greater for the shot with neon injection, indicating an improvement in both calculated and measured momentum confinement with neon injection. For the other "sister shot" pairs with internal transport barriers (102942 and 102940) and with both internal and external transport barriers (106919 and 106972), the improvement of experimental confinement, if any, was less evident and the calculated rotation velocities were relatively insensitive to the neon injection.

In general, the agreement between calculated and measured velocities was quite good, and could certainly be characterized as being "well within a factor of 2" if we exclude the 106xxx shots in which the impurity modeling appeared to be breaking down. This leads us to conclude that neoclassical theory can predict radial transport of toroidal angular momentum to well within a factor of 2 in DIII-D. The general observation of overprediction is probably indicative that a different momentum transport mechanism (in addition to neoclassical) was also involved in the experiments, although refinements in the neoclassical viscosity model and improvements in the ancillary geometric and other modeling approximations could well account for this modest disagreement.

G. Comparison of poloidal rotation velocities

It is instructive to examine some of the intermediate quantities that are calculated from the poloidal momentum balance Eqs. (19)–(21) in order to evaluate the gyroviscous momentum transport frequency of Eq. (12), namely the poloidal velocities and poloidal asymmetry coefficients. The calculated profiles for the deuterium and impurity (carbon) ions poloidal rotation are shown for shot 98777 in Fig. 8(a), together with the measured poloidal rotation profile for carbon VII (here designated $V_{\theta C}^{\Phi}$). The similarity in radial profile for the two calculated rotation velocities was also found for the other shots, except for the lower density 106xxx pair in which a greater difference was found. We note that there are new corrections for geometry and atomic physics which could significantly affect the measured values of poloidal velocity, and for this reason we do not emphasize the comparison of measured and calculated poloidal velocities in this paper, although we plan to undertake such a comparison in the near future.

H. Radial electric fields

The radial electric field predicted using calculated rotation velocities and experimental pressure profiles to evaluate Eq. (24) (without the inertial term) are compared in Fig. 8(b) for shot 98777 with the experimental electric field similarly calculated using the measured rotation velocities and pressure profile for carbon VI. The calculated profile for deuterium used the calculated main ion (deuterium) velocities and measured deuterium pressure profile, while the calculated profile for the impurity species used the calculated velocities for the effective impurity species and the measured carbon VI pressure profile. The calculated and measured values of the radial electric field are in relatively good agreement, with the disagreement arising from the difference in calculated and measured poloidal velocity profiles. Similar, and some-
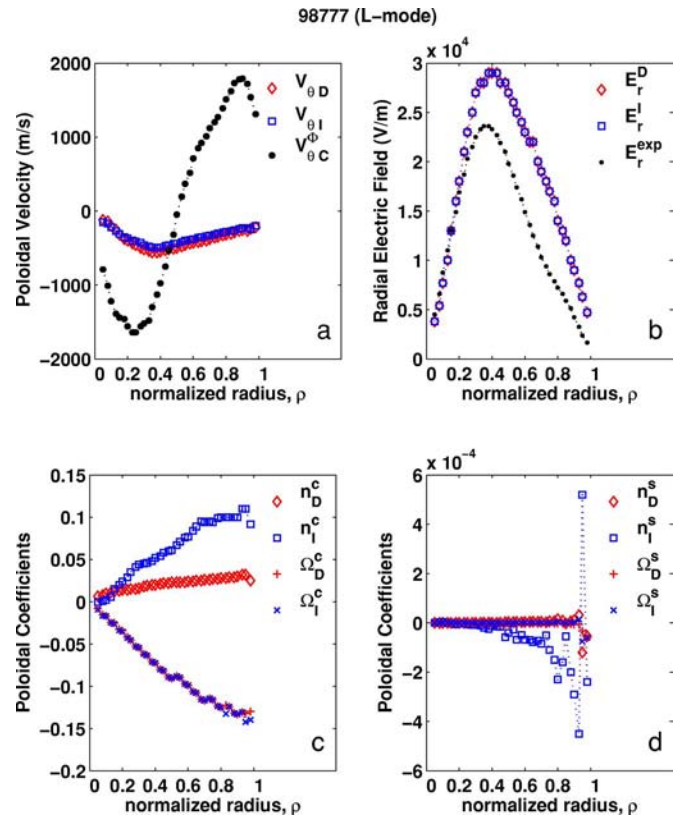

FIG. 8. Intermediate calculated quantities for the *L* mode shot 98777. (a) Poloidal rotation velocities; (b) radial electric field; (c) "in-out" poloidal asymmetry coefficients; (d) "up-down" poloidal asymmetry coefficients. (The experimental poloidal velocity and radial electric field shown are fits to the data.)

times better, agreement was found for the other shots, except for the 106xxx shots (in which the single effective impurity model seemed to break down).

I. Poloidal density and velocity asymmetries

The calculated "in-out" (cosine) and "up-down" (sine) density asymmetries for shot 98777 are shown in Figs. 8(c) and 8(d). The general trends and magnitudes shown in these figures were also found for the other shots, except for the 106xxx shots in which the in-out density asymmetries became larger that unity, indicating a breakdown of the single effective impurity model. The calculated "in-out" density asymmetries increased with radius up to about 15% for the impurity ions (carbon in this shot) and <5% for the deuterium ions. The calculated "in-out" toroidal rotation frequency asymmetries $(\Omega_j^c = V_{\phi j}^c - \varepsilon)$ were similar for deuterium and impurity ions and increased with radius up to −15%. The calculated "up-down" asymmetries were smaller, on the order of 10^{-5} over much of the minor radius, except for the impurity density coefficient which increased up to a few times 10^{-4} at the outer radii. The other shots were similar, except that n_I^c increased only to about 5% for shots 98775 and 99411 but to about 30% for the ITB shots 10294x, and $|n_{i,I}^c| > 1$ for shots 106xxx, which later is unphysical.

We note that the toroidal rotation frequency is frequently assumed to be poloidally uniform in theoretical developments. These calculations indicate that this assumption could introduce errors on the order of as much as 15% in DIII-D.

J. Accuracy of evaluation of gyroviscous angular momentum transfer rate

Since the toroidal rotation velocities are calculated from Eqs. (27) with the densities and the first two terms on the right-hand side taken from experiment and the third beam momentum input term on the right-hand side calculated with some confidence, a comparison of calculated and measured toroidal rotation velocities is really a test of the quantities β_j and of the representation of the interspecies collision frequency ν_{jk}. Assuming the adequacy of the standard form used for the latter, the rotation velocity comparison is a test of the quantities β_j given by Eqs. (28). Since the beam source can be calculated with confidence and the inertial angular momentum transfer frequency given by Eq. (29) was evaluated to be small (but not negligible) in comparison to the gyroviscous angular momentum transfer frequency ν_{dj}, the comparison of measured and calculated toroidal rotation velocities is largely a test of the gyroviscous angular momentum transfer frequency, ν_{dj}. Thus, a brief discussion of the accuracy with which the gyroviscous angular momentum transport rate is represented by the quantity ν_{dj} defined by Eq. (12), as evaluated in this paper, is in order.

The gyroviscous angular momentum transfer rate is rigorously given by Eq. (9). Three approximations are made in reducing Eq. (9) to Eq. (12) that is evaluated for ν_{dj}. First, the cylindrical flux surface geometry approximation $B = B^0/(1 + \varepsilon \cos \theta)$ is made, which certainly introduces some error at the outer radii. Second, the variation of the variables over the flux surface is represented by a low order Fourier expansion, e.g., Eq. (11), based on the observation that in the cylindrical flux surface approximation there is nothing to drive significant higher order asymmetries. Third, the radial derivatives of the asymmetries, e.g., $\partial \tilde{n}_j^{c,s}/\partial r$, are ignored relative to the gradients in the average densities. A limited number of model problem calculations support this third approximation. With these approximations, Eq. (12) is obtained, from which is defined

$$\nu_{dj} \equiv \tfrac{1}{2} \tilde{\theta}_j G_j T_j / R_0^2 e_j B_\phi^0. \tag{33}$$

The accuracy of this expression is determined by the relative magnitude of the errors associated with the three approximations discussed above compared to the magnitude of the composite term, not to the individual components. We believe this expression is accurate in the core of plasmas with toroidal rotation velocities on the order of the corresponding ion sound speeds.

Given the approximations discussed in the previous paragraph, the accuracy of numerically evaluating Eq. (33) for the gyroviscous angular momentum transfer rate comes down to the accuracy of evaluating the various terms in Eq. (33). The terms in the denominator are known quite accurately from experiment, and the experimental ion temperature was used to evaluate the temperature in the numerator.

Experimental gradient scale lengths were used to evaluate the term G_j given by Eq. (14) in order to minimize any uncertainty.

The quantity θ_j given by Eq. (13) depends on toroidal and poloidal velocities and on the density asymmetries $\tilde{n}_j^{c,s}$. The poloidal velocities and the $\tilde{n}_j^{c,s}$ are calculated from the moments of the poloidal momentum balance Eqs. (19)–(21). Note that the $\tilde{\Phi}^{c,s}$ are given in terms of the $\tilde{n}_j^{c,s}$ by Eq. (26). Equations (19)–(21) contain terms through quadratic in the $\tilde{n}_j^{c,s}$, although the quadratic terms were found to have a negligible effect on the solution. The banana-plateau form of the parallel viscosity of Eq. (7) is judged to be an adequate representation in light of current knowledge.[50] The poloidal moments Eqs. (19)–(21) and the toroidal rotation Eqs. (27) are solved as a set of nonlinear equations using standard procedures.

IV. SUMMARY AND CONCLUSIONS

A self-consistent, first-principles formulation of rotation theory based on momentum balance and neoclassical viscosity and its implementation into a calculation model was described and then applied to calculate toroidal rotation velocity profiles in several DIII-D shots in different confinement regimes. The agreement between calculated and measured toroidal rotation velocities was well within a factor of 2 (except in two shots in which an ancillary approximation of the computation model broke down and the agreement was only to within a factor of about 3), and the experimentally observed enhancement of momentum confinement with neon injection was predicted for a pair of L mode shots. The general trend of overprediction of measured toroidal velocities is attributed to a combination of the need for refinements in the neoclassical viscosity representation, ancillary approximations in the calculation model, or to the presence in the experiment of an additional "anomalous" momentum transport or torque input mechanism not included in the calculation model. Future work will address these possibilities.

APPENDIX: A SHORT HISTORY OF GYROVISCOSITY

The calculational model for toroidal rotation and the underlying model for the representation of the gyroviscous toroidal angular momentum transfer rate have evolved over the past 20 years to the form employed in this paper. In the earliest (1985) version[17] the poloidal asymmetry factor $\tilde{\theta}$ of Eq. (13) was estimated to be of the order r/R based on estimates of the impurity density asymmetry. It was subsequently (1987) noted[19] that to leading order in the gyroradius the poloidal asymmetries (and poloidal velocity), hence the gyroviscosity, vanished and that gyroviscosity must be higher order. Subsequent measurements revealed the exis-

tence of poloidal rotation in tokamaks, implying the need to go to higher gyroradius ordering to touch base with experiment. A first principles numerical calculation[20] of poloidal rotation and density asymmetries was made (1992) and employed to evaluate $\tilde{\theta}$ and predict[31] gyroviscous momentum confinement times in general agreement with measured values for several tokamak experiments (1993). These and subsequent calculations indicate that the relatively smaller poloidal asymmetry of the more numerous main ion species dominates the composite $\tilde{\theta}$. Subsequent calculations[33] of poloidal asymmetries and poloidal rotation in DIII-D have led to gyroviscous predictions of momentum confinement times in agreement with experiment for plasmas in several different confinement regimes (2002).

The original Braginski formulation[12] of gyroviscosity (1965), which was extended to develop the formalism used in this paper, was based on the strong rotation ordering $V_\phi \sim V_{\text{th}}$ appropriate for the central regions of the DIII-D plasmas analyzed in this paper and many other beam-injected plasmas. It was noted[16] that in the weak rotation ordering $V_\phi \ll V_{\text{th}}$ it is necessary to retain additional heat flux terms in the gyroviscosity formalism. Although initial extensions[51,22] of the gyroviscous formalism to the steep-gradient edge region (1993–1994) used the Braginski formulation, subsequent work[23,25,27] has included the heat flux terms (2000–2005).

[1] S. Suckewer, H. P. Eubank, R. J. Goldston *et al.*, Phys. Rev. Lett. **43**, 207 (1979).

[2] R. C. Isler, L. E. Murray, E. C. Crume *et al.*, Nucl. Fusion **23**, 1017 (1983).

[3] R. J. Groebner, W. Pfeiffer, F. P. Blau *et al.*, Nucl. Fusion **26**, 543 (1986).

[4] S. D. Scott, V. Arunasalam, C. W. Barnes *et al.*, Phys. Fluids B **2**, 1300 (1990).

[5] H. P. L. deEsch, D. Stork, and H. Weisen, in *Proceedings of the Conference on Controlled Fusion and Plasma Heating, Amsterdam, 1990* (European Physical Society, Geneva, 1990), Vol. 14B, Part I, p. 90.

[6] F. Wagner, F. Ryter, A. R. Field *et al.*, in *Proceedings of the 13th International Conference on Plasma Physics and Controlled Fusion Research, Washington, 1991* (International Atomic Energy Agency, Vienna, 1991), p. 277.

[7] K-D. Zastrow *et al.*, in *Proceedings of the 22nd European Conference on Controlled Fusion and Plasma Physics, Bournemouth, 1995* (European Physical Society, Geneva, 1995), Vol. 19C, Part II, p. 453.

[8] J. S. deGrassie *et al.*, in *Proceedings of the 26th European Conference on Controlled Fusion and Plasma Physics, Maastricht, 1999* (European Physical Society, Geneva, 1999), Vol. 23J, p. 1189.

[9] K-D. Zastrow, W. G. F. Core, L-G. Erickson *et al.*, Nucl. Fusion **38**, 257 (1998).

[10] J. S. deGrassie, D. R. Baker, K. H. Burrell *et al.*, Nucl. Fusion **43**, 142 (2003).

[11] A. N. Kaufmann, Phys. Fluids **3**, 610 (1960).

[12] S. I. Braginskii, Rev. Plasma Phys. **1**, 205 (1965).

[13] M. N. Rosenbluth, P. H. Rutherford, J. B. Taylor *et al.*, in *Proceeding of the Conference on Plasma Physics and Controlled Fusion, Vienna, 1971* (International Atomic Energy Agency, Vienna, 1971), Vol. 1, p. 495.

[14] R. D. Hazeltine, Phys. Fluids **17**, 961 (1974).

[15] K. T. Tsang and E. A. Frieman, Phys. Fluids **19**, 747 (1976).

[16] A. B. Mikhailovskii and V. S. Tsypin, Sov. J. Plasma Phys. **10**, 51 (1984).

[17] W. M. Stacey and D. J. Sigmar, Phys. Fluids **28**, 2800 (1985).

[18] F. L. Hinton and S. K. Wong, Phys. Fluids **28**, 3082 (1985).

[19] J. W. Connor, S. C. Cowley, R. J. Hastie, and L. R. Pan, Plasma Phys. Controlled Fusion **29**, 919 (1987).

[20] W. M. Stacey, Phys. Fluids B **4**, 3302 (1992).

[21] R. D. Hazeltine and J. D. Meiss, *Plasma Confinement* (Addison-Wesley, Reading, 1994), pp. 208, 220, and 226.

[22] A. L. Rogister, Phys. Plasmas **1**, 619 (1994).

[23] H. A. Claassen, H. Gerhauser, and A. Rogister, Phys. Plasmas **7**, 3699 (2000).

[24] W. M. Stacey, Phys. Plasmas **8**, 158 (2001); **9**, 3874 (2002); **11**, 3096 (2004).

[25] P. J. Catto and A. N. Simakov, Phys. Plasmas **11**, 90 (2004); Contrib. Plasma Phys. **44**, 83 (2004).

[26] S. K. Wong and V. S. Chan, Phys. Plasmas **11**, 3432 (2004).

[27] P. J. Catto and A. N. Simakov, Phys. Plasmas **12**, 012501 (2005).

[28] J. J. Ramos, Phys. Plasmas **12**, 112301 (2005).

[29] D. Nishijima, A. Kallenbach, S. Gunter *et al.*, Plasma Phys. Controlled Fusion **47**, 89 (2005).

[30] A. G. Peeters and C. Angioni, Phys. Plasmas **12**, 072515 (2005).

[31] W. M. Stacey and D. R. Jackson, Phys. Fluids B **5**, 1828 (1993).

[32] W. M. Stacey and M. Murakami, Phys. Plasmas **8**, 4450 (2001).

[33] W. M. Stacey and J. Mandrekas, Phys. Plasmas **9**, 1622 (2002).

[34] W. M. Stacey, A. W. Bailey, D. J. Sigmar, and K. C. Shaing, Nucl. Fusion **25**, 463 (1985); W. M. Stacey and D. J. Sigmar, Phys. Fluids **27**, 2076 (1984); **22**, 2000 (1979); Nucl. Fusion **19**, 1665 (1979).

[35] K. H. Burrell, T. Ohkawa, and S. K. Wong, Phys. Rev. Lett. **47**, 511 (1981).

[36] A. Bondeson and D. J. Ward, Phys. Rev. Lett. **72**, 2709 (1994).

[37] M. S. Chu, J. M. Greene, T. H. Jensen, R. W. Johnson *et al.*, Phys. Plasmas **2**, 2236 (1995).

[38] A. M. Garofalo, M. S. Chu, E. D. Fredrickson *et al.*, Nucl. Fusion **41**, 1171 (2001).

[39] E. Hameiri, Phys. Plasmas **5**, 3270 (1998).

[40] K. H. Burrell, Phys. Plasmas **4**, 1499 (1997).

[41] G. R. McKee, M. Murakami, J. Boedo, G. L. Jackson *et al.*, Phys. Plasmas **7**, 1870 (2000); Nucl. Fusion **41**, 317 (2001).

[42] E. J. Doyle, C. M. Greenfield, M. E. Austin *et al.*, Nucl. Fusion **42**, 333 (2002).

[43] M. Murakami, H. St. John, T. A. Caspar *et al.*, Nucl. Fusion **40**, 1257 (2000).

[44] W. P. West, M. R. Wade, C. M. Greenfield *et al.*, Phys. Plasmas **9**, 1970 (2002).

[45] J. Mandrekas, "Physics models and user's guide for the neutral beam module of the SUPERCODE," Georgia Tech Fusion Report No. GTFR-102 (1992), available from National Technical Information Service, NTIS-PB93–121887INZ.

[46] R. J. Goldston, "Topics in confinement analysis of tokamaks with auxiliary heating," in *Basic Physical Processes of Toroidal Fusion Plasmas* (Commission of the European Commission and Monotypia Frachi Citta di Castello, Italy, 1985), Vol. 1, EUR 10418 EN.

[47] W. H. Press, *Numerical Recipes* (Cambridge University Press, Cambridge, 1992).

[48] T. Rowan, "Functional stability analysis of numerical algorithms," Ph.D. thesis, Department of Computer Sciences, University of Texas at Austin (1990), ftp://www.netlib.org/opt/

[49] L. R. Baylor, K. H. Burrell, R. J. Groebner *et al.*, Phys. Plasmas **11**, 3100 (2004).

[50] K-C. Shaing, University of Wisconsin, personal communication (2005).

[51] W. M. Stacey, Phys. Fluids B **5**, 1413 (1993).